Optics Communications 282 (2009) 1728–1733

Contents lists available at ScienceDirect

Optics Communications

journal homepage: www.elsevier.com/locate/optcom

200-Gb/s wavelength conversion using a delayed-interference all-optical semiconductor gate assisted by nonlinear polarization rotation

Jun Sakaguchi [1], Takehiro Nishida, Yoshiyasu Ueno *

University of Electro-Communications, Department of Electronic Engineering, 1-5-1, Chofugaoka, Chofu, Tokyo 182-8585, Japan

ARTICLE INFO

Article history:
Received 14 August 2008
Received in revised form 6 January 2009
Accepted 6 January 2009

Keywords:
All-optical signal processing
Wavelength conversion
Delayed-interference signal-wavelength converter (DISC)
Semiconductor optical amplifier (SOA)
Nonlinear polarization rotation
Pattern-induced intensity fluctuation

ABSTRACT

The pattern-induced intensity fluctuation (PIF) of output signals with a bit-rate above 160 Gb/s has been one of the major issues regarding all-optical semiconductor gates. We have demonstrated that the nonlinear polarization rotation (NPR) in the semiconductor optical amplifier (SOA) plays a significant role in the high-frequency operation of a delayed-interference signal-wavelength converter (DISC). We did this using a cross-correlation system whose temporal resolution is 1.5 ps which was developed to monitor our 200-Gb/s, 4992-bit-long binary-patterned waveforms. When we experimentally optimized the NPR effect inside our DISC specially for our 200-Gb/s wavelength conversion, the PIF was significantly improved (from 5.0 to 1.5, for example). Our systematically measured dependence of the PIF on the polarization settings was qualitatively explained with the new gate model that we developed earlier in this work.

1. Introduction

Ultrafast all-optical signal processors based on cross-phase modulation in semiconductor optical amplifiers (SOAs) continue to draw many researchers' interest as promising key elements in future network systems [1,2]. In particular, signal-wavelength converters are expected to enable ultrafast and low-power-consumption optical cross-connects for use in future optical time division multiplexing-wavelength division multiplexing (OTDM-WDM) networks. Some research groups have demonstrated that error-free wavelength conversion in the frequency range of 160–320 Gb/s is possible using delayed-interference signal-wavelength converters (DISCs) [3–5]. Consequently, a fundamental understanding of the high-frequency gate operation is important.

One major issue concerning SOA-based optical gates including DISCs is pattern-induced intensity fluctuation (PIF). It is widely recognized that the output signal of an SOA gate often suffers from PIF, because the carrier recovery rate in the SOA is relatively slow compared to the operation frequency. So far only two methods to suppress PIF have been reported. One method is to inject a strong holding beam into the SOA [6], which accelerates the carrier recovery through stimulated recombinations; this method contributed to the first demonstration of 160-Gb/s operation [3]. The other method is to detune the bandpass filter (BPF) after the SOA [7–9] and utilize ultrafast chirp dynamics in SOAs; this method was used in the subsequent 160—320-Gb/s experiments [4,5].

Actually, those two are not the only methods to reduce the PIF significantly. One method we report in this paper is to use nonlinear polarization rotation (NPR) in the SOA. NPR has been characterized since 1999 [10–12] and is often used for very low-frequency (2.5—10 Gb/s) all-optical gates in combination with polarizers [13–18]. Researchers have performed 40-Gb/s gating using NPR and a polarizer combined with a detuned filter [19] or a special high-speed SOA [20]. However, possible contributions from the NPR combined with the well known DISC structure have not been studied, to the best of our knowledge. Neither has any experimental study with ultra-high bit-rate signals above 100 Gb/s been reported.

In this paper, we demonstrate that the NPR in the SOA plays a significant role in high-frequency DISC operation, and then propose a design option for suppressing the PIF in such all-optical semiconductor gates. We have performed 200-Gb/s wavelength conversion using a DISC, and investigated how the polarization states of the continuous-wave (cw) light before and after the SOA affect the output PIF through cross-correlation measurements. Systematic results show that we can exploit the NPR to suppress PIF. We speculate that this effect would have possibly contributed to the previous experiments using 160- and 320-Gb/s signals in combination with the other methods.

* Corresponding author. Tel./fax: +81 424435807.
E-mail address: ueno@ee.uec.ac.jp (Y. Ueno).
[1] Present address: Nara Institute of Science and Technology, Ikoma 630-0192, Japan.

0030-4018/$ - see front matter © 2009 Elsevier B.V. All rights reserved.
doi:10.1016/j.optcom.2009.01.028

2. Model of the DISC operation and the NPR effects

In this section, we first describe our model of the DISC operation including NPR effect. Then we show through a numerical simulation that the NPR can be used to suppress PIF.

The original scheme of the DISC gate is shown in Fig. 1a. It consists of one SOA, one Mach–Zehnder interferometer (MZI), and a band-pass filter. The MZI in a practical DISC gate often consists of a set of polarization-control devices. Fig. 1b is a schematic of the DISC gate used in this study, which contains the polarization-based MZI and polarization controllers Q_1 and H_1 placed before it. A rate equation for the carrier density in the SOA active region,

$$\frac{d}{dt}\overline{n_c(t)} = \frac{\eta_T I_{OP}}{qV} - \frac{\overline{n_c(t)}}{\tau_c} - \frac{1}{V}\left(G(\overline{n_c(t)}) - 1\right)\left[\frac{|\mathbf{E}_{pulse}(t)|^2}{h\nu_{pulse}} + \frac{|\mathbf{E}_{CW}|^2}{h\nu_{cw}}\right], \quad (1)$$

has been used for accurate analysis of the DISC output waveforms [2,21]. Here, $\overline{n_c(t)}$ is the average $n_c(z,t)$ over the active region length, $n_c(z,t)$ is the carrier density which contributes to the SOA gain, I_{OP} is the injection current, η_T is the quantum conversion efficiency, τ_c is the carrier lifetime, V is the active region volume, and $\mathbf{E}_{pulse}(t)$ and $\mathbf{E}_{CW}$ are the amplitudes of the control pulse and the cw optical input, respectively. The first, second, and third terms on the right-hand side of Eq. (1), respectively, represent the carrier injection, carrier relaxation, and stimulated recombinations. The chip gain of the SOA is expressed as

$$G(\overline{n_c(t)}) = \exp\left(\Gamma L_{eff}\frac{dg}{dn}\overline{n_c(t)}\right). \quad (2)$$

Here, Γ is the confinement factor, L_{eff} is the effective length of the active region, and dg/dn is the differential gain of the active region. The injection of the control pulse $\mathbf{E}_{pulse}(t)$ instantaneously decreases the carrier density by $\Delta\overline{n_c}$, induces an ultrafast refractive index change of the active region, and causes cross-phase modulation to the cw light.

We then extended our previous DISC model to take the NPR into account. The NPR in the SOA has been primarily attributed to the anisotropy of the refractive index [10–12]. To express it in a simple way, we assumed that the TE and TM components of the input cw light were affected by anisotropic phase shifts:

$$\Phi^{TE}(t) = k_0\Gamma L\frac{dn_r^{TE}}{dn}\Delta\overline{n_c(t)} + \Phi_{eq}^{TE} \quad (3)$$

$$\Phi^{TM}(t) = k_0\Gamma L\frac{dn_r^{TM}}{dn}\Delta\overline{n_c(t)} + \Phi_{eq}^{TM}, \quad (4)$$

respectively. Here, $k_0 = 2\pi\nu_{cw}/c$ is the wave number of the light in vacuum and $dn_r^{TE/TM}/dn$ represents the nonlinear index changes for TE/TM components. $\Phi_{eq}^{TE/TM}$ represents the steady-state anisotropic phases for TE/TM components. Since the relative phase of the TE and TM components after passing through the SOA changes dynamically with t, the polarization state of the combined light rotates accordingly. This polarization rotation results in a dynamic change in the transmittance of the polarizer P_1, and can be used to compensate for the patterning in $G(t)$ and $\Phi(t)$ if we adjust the angles of the

Table 1
Parameter values used in the model calculation.

SOA parameter	Description	Value
I_{op}	Injection current	200 mA
L_{eff}	Active region length (effective)	1100 μm
V	Active region volume	5.2×10^{-11} (cm ^{3})
Γ	Confinement factor	0.2
τ_C	SOA carrier lifetime	75 ps
dg/dn	SOA differential gain	6.36×10^{-16} (cm^2)
η_T	Quantum conversion efficiency	0.34
$\frac{dn_r^{TE}}{dn}$	Refractive index change (TE)	-4.0×10^{-20} (cm^3)
$\frac{dn_r^{TM}}{dn}$	Refractive index change (TM)	-3.0×10^{-20} (cm^3)
Gate parameter	**Description**	**Value**
f	Operation frequency	200 GHz
T_{FWHM}	Input pulse width (FWHM)	1.0 ps
E_{pulse}	Input pulse energy	30 fJ
$P_{cw}\equiv\|\mathbf{E}_{cw}\|^2$	Input cw power	5 mW
Δt	Delay time in the MZI	1.0 ps
ν_{cw}	Frequency of cw light	193.7 THz
ν_{pulse}	Frequency of control pulses	192.8 THz
	PRBS pattern length	2^9-1
$\Delta\Phi_B$	MZI bias	1.0π
Derived parameter	**Description**	**Value**
G_0	Unsaturated SOA gain	37 dB
τ_{eff}	Effective recovery time	10 ps

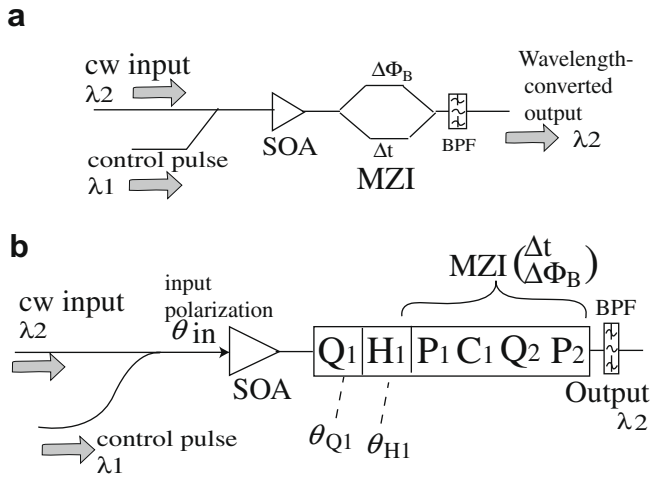

Fig. 1. Schematics of the DISC gate. (a) original DISC scheme and (b) polarization-based DISC scheme in this paper. Q: quarter-waveplate, H: half-waveplate, C: calcite crystal, P: polarizer, BPF: band-pass filter.

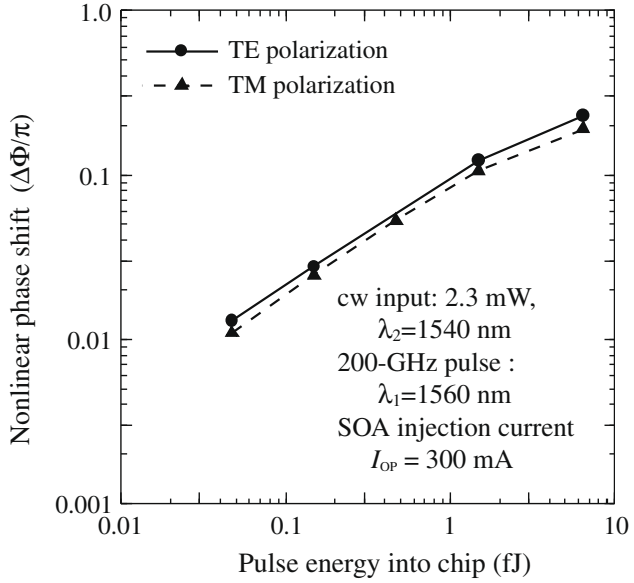

Fig. 2. Measured dependence of the nonlinear phase shift in our SOA for TE/TM-polarized cw light on the input pulse energy.

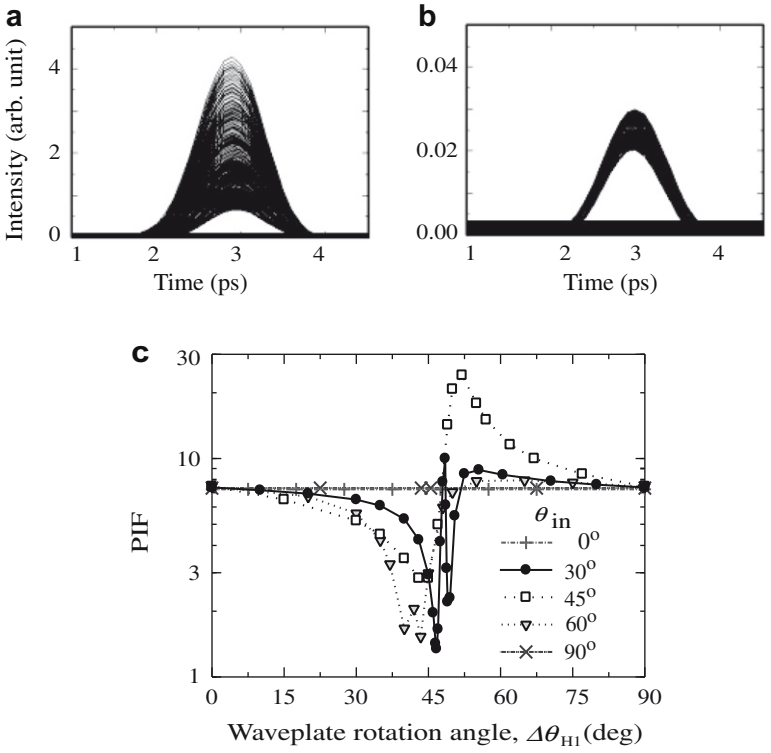

Fig. 3. Calculated DISC output eye diagrams and PIF dependence on the waveplate angle detuning. (a) $\theta_{in} = 0°$, $\Delta\theta_{H_1} = 0°$; (b) $\theta_{in} = 60°$, $\Delta\theta_{H_1} = 40°$; (c) PIF dependences.

quarter waveplate Q_1 and the half-waveplate H_1 adequately. Using Jones vector analysis, we deduced the following expressions for the DISC output power $P_{out}(t)$:

$$P_{out}(t) = |\mathbf{E}_{out}(t)|^2, \tag{5}$$

$$\mathbf{E}_{out}(t) \equiv \mathbf{E}^{TE}_{out}(t)\cos(\theta_{in})A + \mathbf{E}^{TM}_{out}(t)\sin(\theta_{in})B, \tag{6}$$

$$\mathbf{E}^{TE/TM}_{out}(t) \equiv \frac{\mathbf{E}_{cw}}{2}\left[\sqrt{G(t)}\exp\left\{i\left(\Phi^{TE/TM}(t) + \Delta\Phi_B\right)\right\} + \sqrt{G(t-\Delta t)}\exp\left\{i\Phi^{TE/TM}(t-\Delta t)\right\}\right], \tag{7}$$

$$\begin{pmatrix} A \\ B \end{pmatrix} \equiv M_R(-\theta_{Q_1})M_Q M_R(\theta_{Q_1} - \theta_{H_1})M_H M_R(\theta_{H_1})\begin{pmatrix} \cos(\pi/4) \\ \sin(\pi/4) \end{pmatrix}, \tag{8}$$

$$M_R(\theta) \equiv \begin{pmatrix} \cos(\theta) & -\sin(\theta) \\ \sin(\theta) & \cos(\theta) \end{pmatrix}, \quad M_Q = \begin{pmatrix} 1 & 0 \\ 0 & i \end{pmatrix}, \quad M_H = \begin{pmatrix} 1 & 0 \\ 0 & -1 \end{pmatrix}. \tag{9}$$

Here, θ_{in} is the input polarization angle of the cw light into the SOA, θ_{Q_1} is the rotation angle of Q_1, and θ_{H_1} is that of H_1. Δt and $\Delta\Phi_B$ are the delay time and phase bias of the MZI, respectively. The expressions of the amplitude waveforms $\mathbf{E}^{TE/TM}_{out}(t)$ are similar to the conventional expression of the DISC output amplitude.

Using these equations and pseudorandom data inputs, we calculated the DISC output waveforms and their PIFs for several θ_{in} values. Parameter values are summarized in Table 1. To use a realistic value for the refractive index anisotropy, we carefully characterized polarization-dependent nonlinear phase shifts for our SOA sample using a method from [2]. Fig. 2 shows one series of systematically-measured result on the polarization-dependent nonlinear phase shifts. After several measurements, we estimated the refractive index anisotropy for our SOA to be 15—25%, and assumed 25% anisotropy in the model calculation. For each θ_{in} value, we determined the starting values of θ_{Q_1} and θ_{H_1} using only cw input light as follows: we adjusted θ_{Q_1} to eliminate the ellipticity of the cw light, which was caused by the steady-state phases $\Phi^{TE/TM}_{eq}$.[2] θ_{H_1} was chosen so that the polarization axis of the cw light would coincide with the axis of the polarizer P_1. Then we injected data inputs and calculated the output waveform. Fig. 3a shows an example of the calculated eye diagram in such a case ($\theta_{in} = 0°$); a large PIF was observed due to the long effective carrier recovery time ($\tau_{eff} = 10$ ps). In this section, we evaluated the PIF using the intensity ratio of the largest and smallest output pulses, and it was 7.3 for the case of Fig. 3a. After that, we systematically detuned θ_{H_1} from the starting value. θ_{Q_1} was kept unchanged, so that the transmittance of P_1 shifts from maximum to minimum as the detuning $\Delta\theta_{H_1}$ approaches 45°. Then the PIF was suppressed in some cases, as shown in Fig. 3b. Fig. 3c shows the calculated PIF dependence on $\Delta\theta_{H_1}$. When θ_{in} was set to 0° (=TE) or 90° (=TM), the PIF was equal to the standard value (=7.3). In contrast, the PIF values for other θ_{in} settings showed various dependences on $\Delta\theta_{H_1}$. The dependences had a notable feature in common: the PIF values were highly suppressed when $\Delta\theta_{H_1}$ was slightly below 45°. These particular examples show the possibility of an NPR-based PIF suppression method.

3. Waveform-monitoring setup

To demonstrate the significance of NPR in high-frequency DISC operation, we performed a 200-Gb/s wavelength conversion experiment and systematically investigated how the polarization settings before and after the SOA affect the output PIF. We developed a high-resolution, long bit pattern waveform-monitoring system for this purpose because we wanted to evaluate the PIF for a data pattern with certain reality. Fig. 4a gives an overview of the whole setup; 12.48 GHz, 1.6-ps soliton pulses from a mode-locked fiber laser (Pritel Inc., UOC-3) were adiabatically compressed in a dispersion decreasing fiber to 300 fs, and received intensity modulation with a 312-bit data pattern. This pattern was initially determined through a Monte Carlo method. After

[2] Thus Φ^{TE}_{eq} and Φ^{TM}_{eq} affect the starting values of θ_{Q_1} and θ_{H_1} only. They are not essential in the following PIF-suppression scheme.

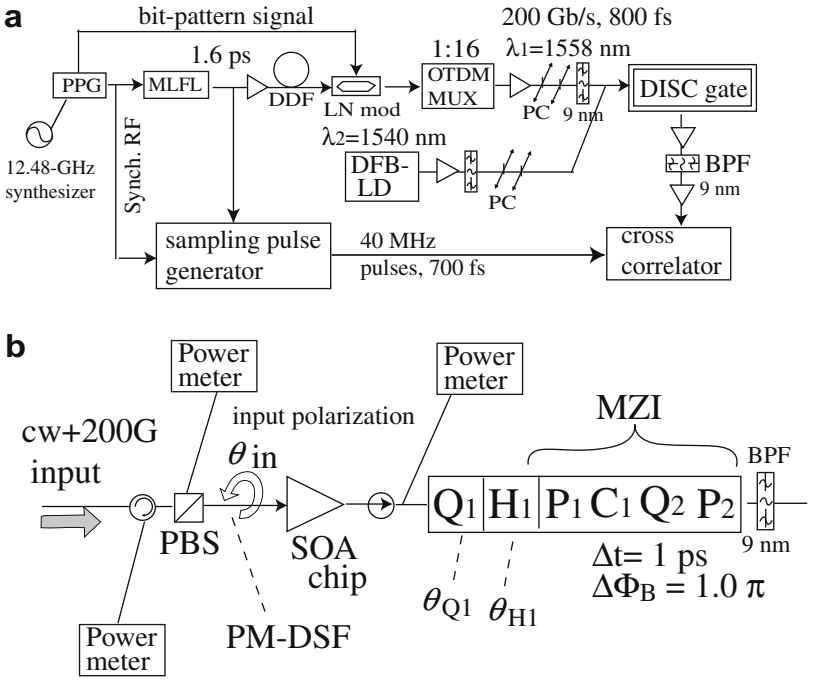

Fig. 4. Experimental setup. (a) Overview, (b) DISC gate based on an SOA chip. PPG: programmable pattern generator, MLFL: mode-locked fiber laser, DDF: dispersion decreasing fiber. PC: polarization controller, PBS: polarization beam splitter, PM-DSF: polarization-maintaining dispersion-shifted fiber.

the modulation, the pulses were multiplexed up to 199.7 Gb/s through four-stage MUXs, received a dispersion compensation, and were used for the gate input signal (width = 800 fs, pattern length = 4992 bits, $\lambda_1 = 1558$ nm). In parallel to that, we generated an ultrafast (700 fs), low-frequency (40 MHz), and high extinction ratio ($\geqslant$27 dB) pulse train for the cross-correlator (Femtochrome Research Inc., FR-103XR) reference input. This pulse train was synchronized to the 200-Gb/s, 4992-bit data input with a low timing jitter, and consequently enabled cross-correlation measurements of the patterned waveform with a time resolution of about 1.5 ps. Details of this pulse generator are explained in [22]. We constructed the DISC gate using a custom-ordered SOA chip, as shown in Fig. 4b. The structure of this SOA chip was designed to be the same as that of the commercially available SOA series. To accurately control the polarization state of the cw light at the SOA input facet, we used a polarization-maintaining dispersion-shifted lensed fiber for the signal input. Monitoring of the ASE intensities on the input and output sides of the SOA enabled on-line coupling adjustments. The MZI was composed of cascaded polarization controllers (Optoquest Inc.), as explained in [21]. The operation parameters are summarized in Table 2. The nonlinear phase shift induced by each control pulse was estimated to be 0.25π for TE component and 0.20π for TM component, respectively, from the separately-measured result in Fig. 2.

Table 2
Summary of experimental conditions.

Gate parameters	Description	Value
f	Operation frequency	199.7 GHz
T_{FWHM}	Input pulse width (FWHM)	0.8 ps
E_{pulse}	Input pulse energy (chip)	7 fJ
P_{cw}	Input cw power (chip)	2.5 mW
Δt	Delay time in the MZI	1.0 ps
λ_{cw}	Wavelength of cw light	1540 nm
λ_{pulse}	Wavelength of control pulses	1558 nm
$\Delta\Phi_B$	MZI bias	1.0π
SOA characteristics	**Description**	**Value**
I_{op}	Injection current	300 mA
P_{op}	DC power consumption	580 mW
G_0	Unsaturated SOA gain	33.6 dB
τ_C	SOA carrier lifetime	42 ps
E_{sat}	Saturation energy for pulse	400 fJ

4. PIF measurement results

We monitored the input and output waveforms of the DISC gate using the cross-correlation method. Since the time span of the cross-correlator was limited to about 180 ps, we could monitor only a short segment of the 4992-bit-long waveform with one scan. Fig. 5a shows two particular segments of the input waveform. We could monitor another segment in another scan, by shifting the 12.48-Gb/s encoding pattern properly. The two examples in the figure show a '0-dominant' part ('0000100000000001') and '1-dominant' part ('11101011111111'), respectively. As shown in this figure, the longest interval between two '1' bits and that for two '0' bits was 55 and 45 ps, respectively. Note that the $2^7 - 1$-bit pseudorandom data pattern used in the past 160—320 Gb/s demonstrations contained only 6—7 successive '0' and '1'. Considering that the typical effective recovery time of our SOA was within 40–15 ps (for holding-beam power of 0.001–12 mW), we assert that our measurement provided more stringent PIF evaluation.

Fig. 5b shows the corresponding segments of the DISC output waveform when there was no NPR in the SOA ($\theta_{in} = 0^\circ$). In this case, we see that the intensity of the output signal after the successive '0' bits is large compared to that at the end of the successive '1' bits. We evaluated the PIF to be 5.0, using the ratio of the largest and smallest pulse intensities. We systematically rotated the H_1 angle, but no significant PIF improvement was observed. The situation was almost the same when we changed the input polarization state from TE to TM ($\theta_{in} = 90^\circ$).

The situation changed when we aligned the input polarization to $\theta_{in} = 30^\circ$, which lay between the TE and TM axes. When we maximized the transmittance of P_1 by adjusting θ_{Q_1} and θ_{H_1}, the

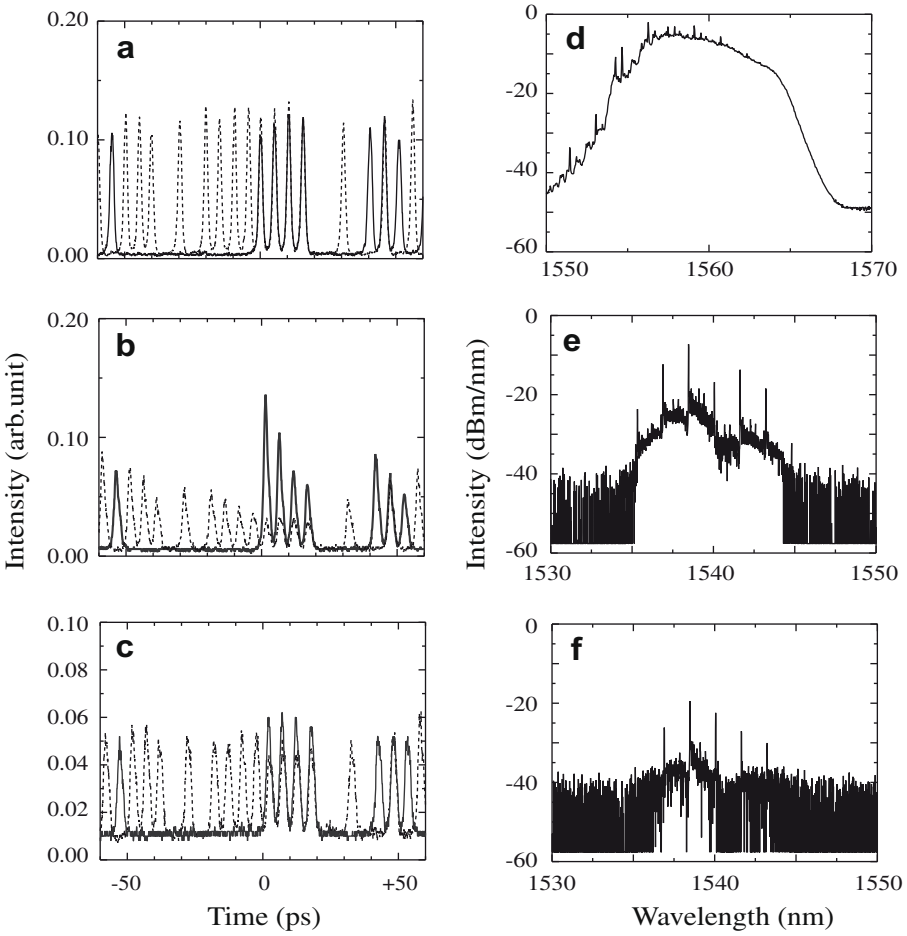

Fig. 5. Measured 200-Gb/s digital signal waveforms and spectra. (a) Input waveforms, (b) output waveforms ($\theta_{in} = 0°$, $\Delta\theta_{H_1} = 0°$), (c) output waveforms ($\theta_{in} = 30°$, $\Delta\theta_{H_1} = 42°$), (d)–(f) corresponding spectra. The solid traces and dashed traces in (a)–(c) show '0'-dominant parts and '1'-dominant parts of the 4992-bit patterned waveforms, respectively.

PIF value was almost the same as before. As we detuned θ_{H_1} after that, the output PIF was drastically reduced (=1.5) as shown in Fig. 5c. Furthermore, no significant signal degradation due to subpulse generation was observed [21]. It was potentially due to unexpected contribution from carrier heating in the SOA, but we do not have definite answer at the moment. The spectra of the signals corresponding to Fig. 5a–c are shown in Fig. 5d–f, respectively.

We systematically measured the dependence of the PIF on $\Delta\theta_{H_1}$ at several input polarization states to the SOA. The results are shown in Fig. 6a. When θ_{in} was 30°, the PIF was suppressed around $\Delta\theta_{H_1} = 30$—$42°$. A similar reduction of the PIF below $\Delta\theta_{H_1} < 45°$ was obtained for $\theta_{in} = 45°$, though within a narrower $\Delta\theta_{H_1}$ range. From the similarity of the measured PIF-suppression profiles and the calculated ones in Section 2, we consider that we obtained convincing proof of the NPR-based PIF suppression.

One drawback of this NPR-based PIF-suppression method is the fairly large decrease in the average output power of the DISC. Fig. 6b shows the dependence of the average output power on $\Delta\theta_{H_1}$. As we approach the region where large PIF suppression occurs, the average output power tends to decrease because of the reduced transmittance of P_1. When we obtained the waveform shown in Fig. 5c, the average output power decreased from −15.3 to −26.4 dBm. Nonetheless, Fig. 5b and c indicate that the weak pulses in the patterned output signals were not seriously degraded after the PIF suppression. Fig. 6c shows the dependence of the extinction ratio, which we defined by the intensity ratio of the smallest pulse and the background noise, on $\Delta\theta_{H_1}$. The extinction ratio for Fig. 5c was 3.2, and not decreased much from that for Fig. 5b (=3.8).[3] We consider that this method in proper combination with other PIF-suppression methods (holding-beam injection and BPF detuning) will reduce the drawback on the output power, and enable more efficient operation of DISCs and also other kinds of SOA-based all-optical gates.

5. Conclusion

We systematically measured the pattern-induced intensity fluctuation (PIF) of a wavelength-converted signal from a DISC at 200 Gb/s, and investigated how the nonlinear polarization rotation (NPR) in the SOA affected the PIF. By detuning the polarization angle of the cw light at the SOA input facet from its TE axis ($\theta_{in} = 30°$, for example) and rotating the half-waveplate before the MZI by a certain degree ($\Delta\theta_{H_1} = 30$—$42°$), we could suppress the PIF from 5.0 to 1.5 without using a strong holding beam or band-pass filter detuning. Our DISC model including the NPR effect qualitatively explained the observed PIF-suppression characteristics below $\Delta\theta_{H_1} < 45°$. Thus, we conclude that the NPR in the SOA plays a significant role in the high-frequency operation of the DISC gate, and that it can be used for PIF suppression. We speculate that this effect

[3] These values were fairly small, mostly because of large ASE noise from the EDFA just before the cross-correlator input (Fig. 4a). We expect that the extinction ratio of the DISC output signal before amplification was much higher, but we could not evaluate it because of our experimental limitation.

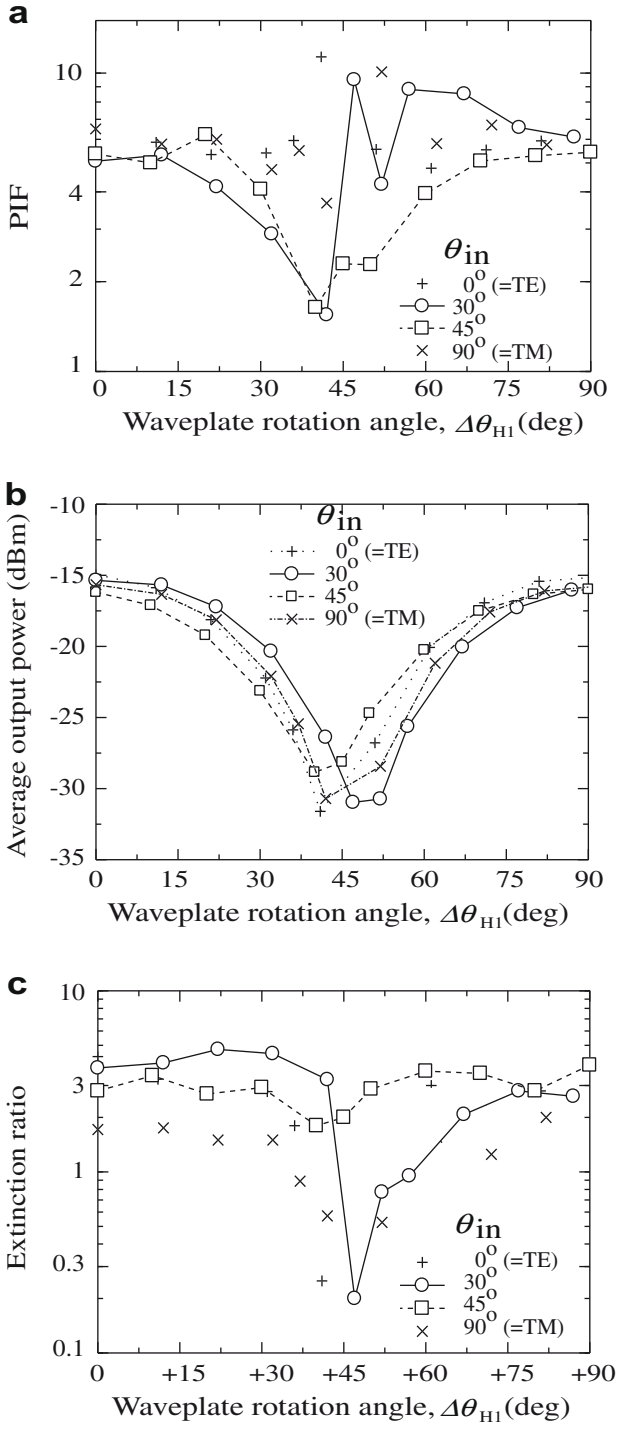

Fig. 6. Measured dependences of (a) PIF, (b) output power, and (c) extinction ratio on the waveplate angle detuning.

would have considerably contributed to the results in past 160—320-Gb/s wavelength conversion experiments [3–5]. We expect this NPR-assisted PIF-suppression method to provide new design options not only for DISCs but also for various other kinds of SOA gate.

Acknowledgements

We thank Dr. Kohsuke Nishimura of KDDI Research Laboratories for the design and fabrication of the custom-ordered SOA chips. We also thank Mr. Takeru Yamaji and Mr. Hiroyuki Takeuchi for the supplemental characterization of the anisotropic nonlinear phase shift in the SOA. This research was supported by the research project grant, "Ultra-low-power and ultrafast optical memory/switching device, of the New Energy and Industrial Technology Development Organization (NEDO), and the 21st-Century University's Center of Excellence (COE) program, "Innovation in coherent optical science, of the University of Electro-Communications, Japan.

References

[1] K.E. Stubkjaer, IEEE J. Sel. Top. Quant. Electron. 6 (2000) 1428.
[2] Y. Ueno, S. Nakamura, K. Tajima, J. Opt. Soc. Am. B19 (2002) 2573.
[3] S. Nakamura, Y. Ueno, K. Tajima, IEEE Photonics Technol. Lett. 13 (2001) 1091.
[4] Y. Liu, E. Tangdiongga, Z. Li, S. Zhang, H. de Waardt, G.D. Khoe, H.J.S. Dorren, J. Lightwave Technol. 24 (2006) 230.
[5] Y. Liu, E. Tangdiongga, Z. Li, H. de Waardt, A.M.J. Koonen, G.D. Khoe, X. Shu, I. Bennion, H.J.S. Dorren, J. Lightwave Technol. 25 (2007) 103.
[6] R.J. Manning, D.A.O. Davies, Opt. Lett. 19 (1994) 889.
[7] M.L. Nielsen, J. Mørk, J. Opt. Soc. Am. B21 (2004) 1606.
[8] M.L. Nielsen, J. Mørk, R. Suzuki, J. Sakaguchi, Y. Ueno, Opt. Express 14 (2006) 331.
[9] J. Wang, A. Marculescu, J. Li, P. Vorreau, S. Tzadok, S.B. Ezra, S. Tsadka, W. Freude, J. Leuthold, IEEE Photonics Technol. Lett. 19 (2007) 1955.
[10] H. Soto, D. Erasme, G. Guekos, IEEE Photonics Technol. Lett. 11 (1999) 970.
[11] R.J. Manning, A. Antonopoulos, R. Le Roux, A.E. Kelly, Electron. Lett. 37 (2001) 229.
[12] H.J.S. Dorren, A.K. Mishra, X. Yang, Z. Li, H. Ju, H. de Waardt, D. Khoe, D. Lenstra, Jpn. J. Appl. Phys. 43 (2004) 5731.
[13] M.F.C. Stephens, M. Asghari, R.V. Penty, I.H. White, IEEE Photonics Technol. Lett. 9 (1997) 449.
[14] H. Soto, J.D. Topomondzo, D. Erasme, M. Castro, Opt. Commun. 218 (2003) 243.
[15] M. Zhao, J. DeMerlier, G. Morthier, R. Baets, IEEE Photonics Technol. Lett. 15 (2003) 305.
[16] Y. Liu, M.T. Hill, E. Tangdiongga, H. de Waardt, N. Calabretta, G.D. Khoe, H.J.S. Dorren, IEEE Photonics Technol. Lett. 15 (2003) 90.
[17] L.Q. Guo, M.J. Connelly, J. Lightwave Technol. 23 (2005) 4037.
[18] J. Zhang, J. Wu, C. Feng, K. Xu, J. Lin, IEEE Photonics Technol. Lett. 19 (2007) 33.
[19] J. Zhang, J. Wu, C. Feng, K. Xu, J. Lin, Electron. Lett. 42 (2006) 970.
[20] G. Contestabile, N. Calabretta, M. Presi, E. Ciaramella, IEEE Photonics Technol. Lett. 17 (2005) 2652.
[21] J. Sakaguchi, M.L. Nielsen, T. Ohira, R. Suzuki, Y. Ueno, Jpn. J. Appl. Phys. 47 (2008) 7182.
[22] J. Sakaguchi, PhD dissertation, University of Electro-Communications, 2008.